Applied Catalysis A: General 469 (2014) 466–471

Contents lists available at ScienceDirect

Applied Catalysis A: General

journal homepage: www.elsevier.com/locate/apcata

Hydrogenation of succinic acid to tetrahydrofuran (THF) over ruthenium–carbon composite (Ru–C) catalyst

Ung Gi Hong, Jeong Kwon Kim, Joongwon Lee, Jong Kwon Lee, Ji Hwan Song, Jongheop Yi, In Kyu Song*

School of Chemical and Biological Engineering, Institute of Chemical Processes, Seoul National University, Shinlim-dong, Kwanak-ku, Seoul 151-744, South Korea

ARTICLE INFO

Article history:
Received 11 July 2013
Received in revised form 12 October 2013
Accepted 15 October 2013
Available online 27 October 2013

Keywords:
Hydrogenation
Succinic acid
Tetrahydrofuran
Ruthenium
Mesoporous carbon

ABSTRACT

Ruthenium–carbon composite (Ru–*X*C) catalysts prepared by a single-step surfactant-templating method were pre-graphitized at different temperature (*X* = 200, 250, 300, 350, and 400 °C), and they were applied to the liquid-phase hydrogenation of succinic acid to tetrahydrofuran (THF). The effect of pre-graphitization temperature on the catalytic performance of Ru–*X*C catalysts (*X* = 200, 250, 300, 350, and 400 °C) was investigated. It was observed that Ru–*X*C composite catalysts showed different textural properties depending on pre-graphitization temperature. In the liquid-phase hydrogenation of succinic acid to tetrahydrofuran (THF), conversion of succinic acid and yield for THF showed volcano-shaped trends with respect to pre-graphitization temperature. In other words, an optimal pre-graphitization temperature was required to achieve maximum catalytic performance of Ru–*X*C catalysts. Yield for THF in the hydrogenation of succinic acid increased with decreasing ruthenium particle size of Ru–*X*C catalysts. Among the catalysts tested, Ru-300C, which had the smallest ruthenium particle size, showed the highest yield for THF.

1. Introduction

Tetrahydrofuran (THF) is a very important chemical in various polymer industries. THF can be converted into polytetramethylene ether glycol (PTMEG) and tetrahydrothiophene [1–3]. THF is also widely used as a solvent in the production of polyvinyl chloride (PVC) and paints. THF is currently produced via several petrochemical processes such as hydrogenation of maleic anhydride (MAN) [4], dehydration of 1,4-butanediol (BDO) [5], and oxidation of butadiene (BD) [6]. However, all these feedstocks (MAN, BDO, and BD) are obtained from fossil fuels, leading to several problems such as unstable price and environmental contamination. Therefore, demand for finding a new and clean platform that can replace these feedstocks has continuously increased [7–9].

Recently, conversion of succinic acid to THF has attracted much attention, because of the increase of succinic acid production in the biorefinery process [10,11]. Succinic acid is a cheap and bio-based chemical that can be converted into THF by hydrogenation reaction. It is known that ruthenium-based catalyst is one of the efficient catalysts for selective formation of THF through hydrogenation of succinic acid [12–14]. Many researches on ruthenium catalysts have been focused on finding suitable supporting materials. Among various supporting materials, carbon has been widely employed due to its well-developed porosity, non-toxicity, and hydrophobic property [15–17].

We have previously investigated the liquid-phase hydrogenation of succinic acid over novel metal catalyst impregnated on mesoporous carbon prepared by a surfactant-templating method [14,18]. We found that carbon support prepared by a surfactant-templating method retained high surface area and large pore volume, leading to excellent physical properties. For this reason, novel metal catalyst impregnated on mesoporous carbon showed a considerable catalytic performance in the hydrogenation of succinic acid to THF [18]. However, novel metal catalyst impregnated on mesoporous carbon required a number of filtration and drying steps. Furthermore, novel metal particles did not well interact with carbon framework.

It has been reported that structure of carbon framework prepared by a self-assembly method can be controlled by pre-graphitization treatment [19,20]. If metal–carbon interaction is properly formed, therefore, metal dispersion of metal–carbon composite prepared by a single-step surfactant-templating method may be controlled. In other words, metal particle size of metal–carbon composite can be controlled by changing pre-graphitization temperature. Furthermore, metal–carbon composite prepared by a single-step surfactant-templating method with pre-graphitization can not only achieve a fine metal dispersion but also provide a simple preparation route. Therefore, it is

* Corresponding author. Tel.: +82 2 880 9227; fax: +82 2 889 7415.
E-mail address: inksong@snu.ac.kr (I.K. Song).

0926-860X/$ – see front matter © 2013 Elsevier B.V. All rights reserved.
http://dx.doi.org/10.1016/j.apcata.2013.10.029

expected that ruthenium–carbon composite prepared by a single-step surfactant-templating method can serve as an excellent catalyst in the hydrogenation of succinic acid to THF, if it is properly pre-graphitized.

In this work, ruthenium–carbon composite (Ru–*X*C) catalysts prepared by a single-step surfactant-templating method were pre-graphitized at various temperatures (*X* = 200, 250, 300, 350, and 400 °C) to control carbon structure and ruthenium dispersion. The Ru–*X*C composite catalysts were characterized by N_2 adsorption–desorption isotherm, XRD, HR-TEM, and EDX, CO chemisorption analyses. Liquid-phase hydrogenation of succinic acid to THF was carried out over Ru–*X*C catalysts in a batch reactor. The effect of pre-graphitization temperature on the textural properties and catalytic activities of Ru–*X*C catalysts was investigated.

2. Experimental

2.1. Preparation of ruthenium–carbon composite catalysts

Fig. 1 shows the schematic procedures for the preparation of ruthenium–carbon composite (Ru–*X*C, *X* = 200, 250, 300, 350, and 400 °C) catalysts. A carbon precursor (sucrose, 8 g, Aldrich), P123 (tri-block copolymer surfactant, 16 g, Aldrich), and ruthenium precursor ($RuCl_3$, 1.3 g, Kojima chemical) were dissolved in 4 M HCl solution (300 ml) at 40 °C for 4 h under stirring. After a silica precursor (TEOS, 36 ml, Aldrich) was slowly added into the solution, the mixture was constantly stirred for 3 h. After the mixture was dried at 100 °C for 48 h, the resulting brown powder was calcined at various temperatures (200, 250, 300, 350, and 400 °C) for 4 h at a heating rate of 5 °C/min in a nitrogen stream (100 ml/min) for pre-graphitization. The calcined powder was then washed and filtered with de-ionized water, and subsequently, it was dried at 80 °C to obtain a ruthenium/carbon slurry/silica composite. For the complete dehydration of surfactant, 2 g of composite was treated with 40 ml of 0.4 M H_2SO_4 solution for 12 h. The resulting brown solid was then carbonized at 800 °C for 4 h at a heating rate of 5 °C/min in a nitrogen stream (100 ml/min). The resultant was further treated with 5 wt% HF solution to remove silica template. After it was dried overnight at 80 °C, the dried ruthenium–carbon composite was reduced with a mixed stream of hydrogen (2.5 ml/min) and nitrogen (47.5 ml/min) at 450 °C prior to the catalytic reaction. The ruthenium–carbon composite catalysts pre-graphitized at different temperature (200, 250, 300, 350, and 400 °C) were denoted as Ru–*X*C (Ru-200C, Ru-250C, Ru-300C, Ru-350C, Ru-400C), where *X* represented the pre-graphitization temperature in Celsius.

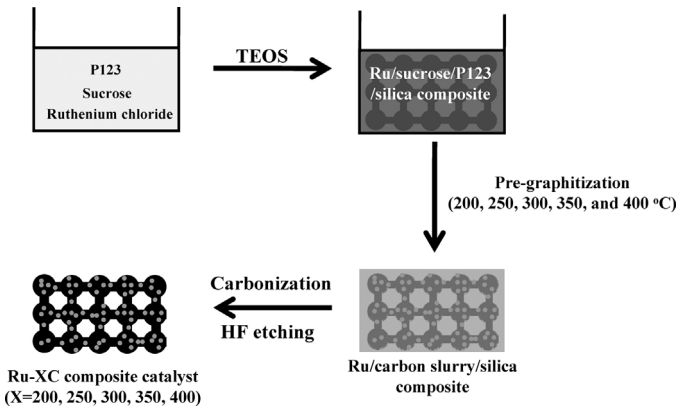

Fig. 1. Schematic procedures for the preparation of Ru–*X*C composite catalysts.

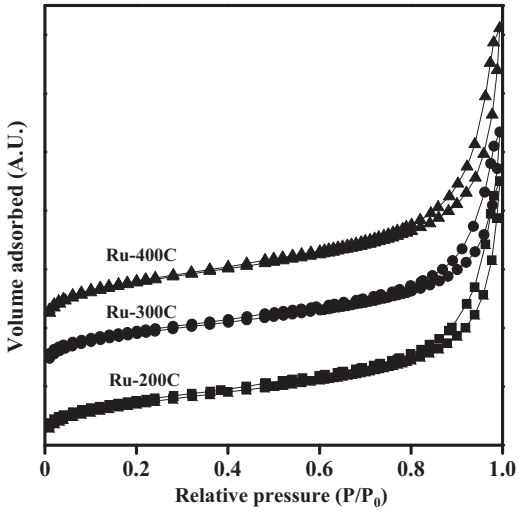

Fig. 2. Nitrogen adsorption–desorption isotherms of Ru–*X*C catalysts reduced at 450 °C.

2.2. Characterization

Nitrogen adsorption–desorption isotherms of ruthenium–carbon composite (Ru-200C, Ru-300C, and Ru-400C) catalysts were obtained with an ASAP-2010 instrument (Micromeritics). Surface areas and pore volumes of the composite catalysts were calculated using the BET equation and the BJH model, respectively. XRD patterns of Ru–*X*C catalysts were obtained with a Rigaku D-Max2500-PC instrument using Cu-Kα radiation (λ = 1.541 Å) operated at 50 kV and 100 mA. Ruthenium dispersion was examined by HR-TEM (Jeol, JEM-3000F), EDX (Tecnai F20, FEI), and CO chemisorption (BELCAT-B, BEL Japan) analyses.

2.3. Hydrogenation of succinic acid to THF

Liquid-phase hydrogenation of succinic acid (SA) to THF was carried out over Ru–*X*C catalysts (*X* = 200, 250, 300, 350, and 400 °C) in a batch reactor at 240 °C and 80 bar (H_2). Succinic acid (0.5 g) and a reduced Ru–*X*C catalyst (0.2 g) were charged into an autoclave (150 ml). 1,4-Dioxane (50 ml) was used as a solvent for the reaction. The reactor was purged with nitrogen to remove air, and then it was pressurized up to 40 bar using hydrogen. After heating the reactor to reaction temperature (240 °C), hydrogen pressure was raised up to 80 bar. The catalytic reaction was carried out for 4 h. During the reaction, reaction mixture was stirred at 500 rpm in order to avoid mass transfer limitation. Reaction products were analyzed using a gas chromatograph (Younglin, ACME-6100) equipped with a FID (flame ionization detector). In order to investigate the stability of the catalyst after the reaction, the amount of ruthenium leaching was measured by ICP-AES (PerkinElmer, Optima-4300DV) analyses.

3. Results and discussion

3.1. Textural properties of Ru–XC catalysts

Fig. 2 shows the nitrogen adsorption–desorption isotherms of Ru–*X*C (*X* = 200, 300, and 400 °C) catalysts. All the Ru–*X*C catalysts showed type-IV isotherm and type-H4 hysteresis loop. With increasing pre-graphitization temperature, more apparent type-H4 hysteresis loop indicating the existence of micropore-like mesopores [21] was observed.

Textural properties of Ru–*X*C (*X* = 200, 250, 300, 350, and 400 °C) catalysts are summarized in Table 1. Average pore size of Ru–*X*C

Table 1
Textural properties of Ru–*X*C catalysts.

	Surface area (m^2/g-cat.)	Micropore surface area ($S_{micropore}$) (m^2/g-cat.)	$S_{micropore}/S_{mesopore}$	Pore volume (cm^3/g-cat.)	Average pore size (nm)
Ru-200C	412	193	0.47	0.69	6.8
Ru-250C	430	221	0.51	0.72	6.7
Ru-300C	472	258	0.55	0.74	6.3
Ru-350C	533	311	0.58	0.78	6.0
Ru-400C	574	362	0.63	0.87	5.7

catalysts was in the mesopore range (5.7–6.8 nm), and average pore size of Ru–*X*C catalysts gradually decreased with increasing pre-graphitization temperature. Surface area and pore volume of Ru–*X*C catalysts increased with increasing pre-graphitization temperature. It has been reported that surface area of carbon increases with increasing pre-graphitization temperature due to the increase of micropore formed by thermal activation [19,22]. Therefore, surface area and pore volume of Ru–*X*C catalysts increased with increasing pre-graphitization temperature, while average pore size of Ru–*X*C catalysts decreased with increasing pre-graphitization temperature. The ratio of micropore surface area with respect to mesopore surface area of Ru–*X*C catalysts also increased with increasing pre-graphitization temperature. This indicates that pre-graphitization at high temperature may cause destruction of mesopore, leading to the increase of microporosity.

3.2. Crystalline structure and ruthenium dispersion of Ru–*X*C catalysts

Fig. 3 shows the XRD patterns of unreduced and reduced Ru–*X*C (*X* = 200, 250, 300, 350, and 400 °C) catalysts. It was observed that all the Ru–*X*C catalysts exhibited a weak shoulder at $2\theta = 25°$, which was attributed to graphitic carbon [23]. Unreduced Ru–*X*C catalysts showed the characteristic XRD peaks of metallic ruthenium ($2\theta = 38°$, 42°, 44°, and 58°), bulk ruthenium oxide ($2\theta = 28°$, 34°, and 57°), and ruthenium chloride ($2\theta = 48°$) [24]. This means that washing step and carbonization step were not sufficient to form complete metallic ruthenium. On the other hand, the reduced Ru–*X*C catalysts did not show XRD peaks of ruthenium oxide or ruthenium chloride but showed metallic ruthenium peaks at $2\theta = 38°$, 42°, 44°, and 58°. These results indicate that ruthenium species in the Ru–*X*C catalysts were completely reduced into metallic ruthenium during the reduction process.

It was also observed that ruthenium peak intensity of reduced Ru–*X*C catalysts decreased in the order of Ru-200C > Ru-400C > Ru-350C > Ru-250C > Ru-300C. This result indicates that ruthenium particles of Ru-300C catalyst were most finely dispersed on the carbon framework. In general, dispersion of ruthenium catalyst supported on metal oxide is determined by hydrogen chemisorption measurement [25]. In case of ruthenium catalyst with carbon material, however, it was difficult to determine the accurate dispersion of ruthenium due to considerable hydrogen spillover to carbon material [26–28]. In order to determine the accurate dispersion of ruthenium in the Ru–*X*C catalysts, therefore, particle size of ruthenium was calculated by Debye–Scherrer equation (using XRD peaks) [29,30] and CO chemisorptions.

Table 2 shows the average ruthenium particle sizes of Ru–*X*C catalysts determined by XRD and CO chemisorption measurements. Ruthenium particle sizes of Ru–*X*C catalysts determined by XRD and CO chemisorption measurements showed the same trend with respect to pre-graphitization temperature. In the Ru–*X*C catalysts (*X* = 200, 250, and 300 °C), ruthenium particle size became smaller with increasing pre-graphitization temperature. In other words, ruthenium particle size became smaller with increasing interaction between ruthenium and carbon framework. This might be explained by metal sintering resistance [31–33]. With a stronger ruthenium–carbon interaction, Ru–*X*C catalysts (*X* = 200, 250, and 300 °C) showed a stronger resistance toward ruthenium sintering, resulting in smaller particle size of ruthenium. In case of Ru–*X*C catalysts (*X* = 300, 350, and 400 °C), however, ruthenium particle size became larger with increasing pre-graphitization temperature, due to collapse of mesopore. Pre-graphitization at high temperature provides not only strong ruthenium–carbon interaction but also increase of micropore. As presented in Table 1, the ratio of micropore surface area with respect to mesopore surface area of Ru–*X*C (*X* = 300, 350 and 400 °C) catalysts increased with increasing pre-graphitization temperature. In other words, mesoporosity of Ru–*X*C decreased with increasing pre-graphitization temperature. It is known that mesoporosity is also responsible for enhancing dispersion of metal particle in the metal-support system [18]. Although Ru-350C and Ru-400C retained stronger interaction between ruthenium and carbon framework than Ru-300C, therefore, they did not show smaller ruthenium particle size than Ru-300C. These results indicate that both ruthenium–carbon interaction and mesoporosity of Ru–*X*C catalysts are responsible for achieving fine dispersion of ruthenium incorporated with carbon framework. Thus, an optimal pre-graphitization temperature for the treatment of Ru–*X*C was required to yield small ruthenium particles.

Table 2
Ruthenium particle sizes of Ru–*X*C catalysts.

	Ruthenium particle size (nm) determined by XRD[a]	Ruthenium particle size (nm) determined by CO chemisorption	Ruthenium particle size (nm) determined by HR-TEM
Ru-200C	10.4	15.1	14.3
Ru-250C	4.9	6.0	6.0
Ru-300C	3.6	4.8	3.3
Ru-350C	5.5	6.3	6.5
Ru-400C	7.7	13.7	10.6

[a] Calculated using the Debye–Scherrer equation.

Fig. 4 shows the HR-TEM images of Ru–*X*C catalysts (*X* = 200, 250, 300, 350, and 400 °C) reduced at 450 °C. In the Ru–*X*C catalysts (*X* = 200, 250, and 300 °C), ruthenium particle size became smaller with increasing pre-graphitization temperature. In the Ru–*X*C catalysts (*X* = 300, 350, and 400 °C), however, ruthenium particle size became larger with increasing pre-graphitization temperature. In order to ensure the trend of ruthenium particle size of Ru–*X*C catalysts, sizes of 200 metallic ruthenium particles in the reduced catalysts were directly measured from HR-TEM images, as summarized in Table 2. It was observed that the trend of average ruthenium particle size determined by HR-TEM was well consistent with the trend of ruthenium particle size determined by XRD and CO chemisorption. Among the Ru–*X*C catalysts, Ru-300C catalyst showed the smallest ruthenium particles (less than 5 nm), while Ru-200C catalyst showed the largest ruthenium particle size (above 10 nm).

Fig. 5 shows the enlarged HR-TEM image of Ru-300C catalyst and its EDX image obtained by mapping on ruthenium. TEM result

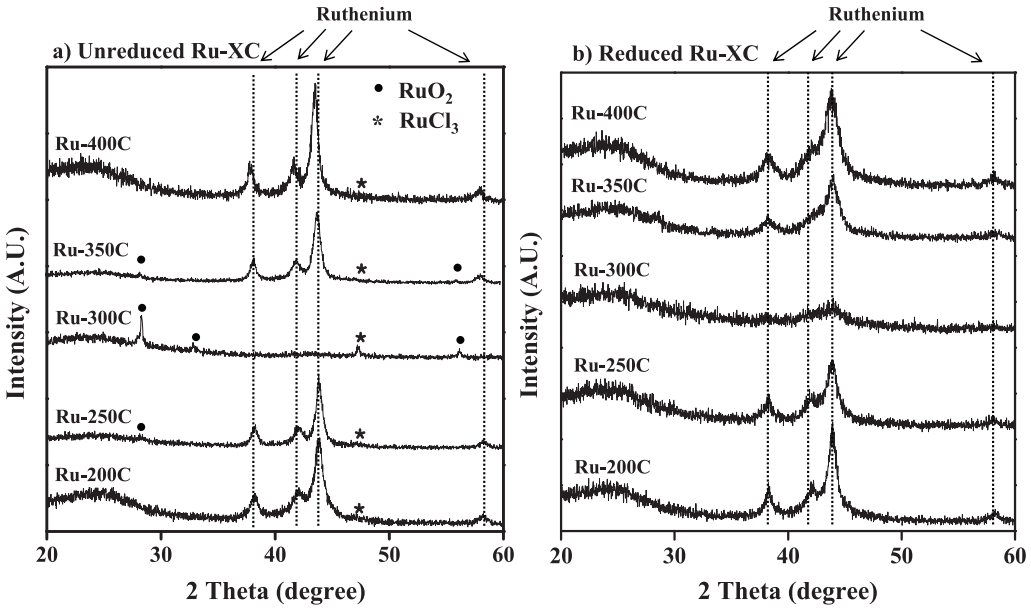

Fig. 3. XRD patterns of (a) unreduced and (b) reduced Ru–*XC* catalysts.

shows that small ruthenium particles (less than 4 nm) were well incorporated on the carbon framework in the Ru-300C composite catalyst. EDX image of Ru-300C catalyst obtained by mapping on ruthenium also clearly supports that ruthenium was finely dispersed on the carbon support.

3.3. Hydrogenation of succinic acid to THF over Ru–XC catalysts

Catalytic performance of Ru–*XC* catalysts (*X* = 200, 250, 300, 350, and 400 °C) in the liquid-phase hydrogenation of succinic acid to THF is shown in Fig. 6. THF (41–51% selectivity) together with γ-butyrolactone (24–36% selectivity) and 1,4-butanediol (6–8% selectivity) were produced as main products via hydrogenation of succinic acid. Ethanol was produced as a major by-product via hydrogenolysis and oxidative-hydrogenation of succinic acid, and small amounts of acetic acid and butyric acid were also produced as by-products. It is known that ruthenium is one of the most efficient catalysts for hydrogenolysis and oxidative-hydrogenation [34,35]. Therefore, the side reaction (formation of ethanol) competitively occurred together with hydrogenation of succinic acid (formation of THF) over the ruthenium–carbon composite catalyst. As shown in Fig. 6, it should be noted that both conversion of succinic acid and yield for THF showed volcano-shaped trends with respect to pre-graphitization temperature. This means that an optimal pre-graphitization temperature was required for maximum production of THF. Among the catalyst tested, Ru-300C catalyst showed the highest conversion of succinic acid (91.2%) and the highest yield for THF (46.4%), while Ru-200C catalyst showed the lowest conversion

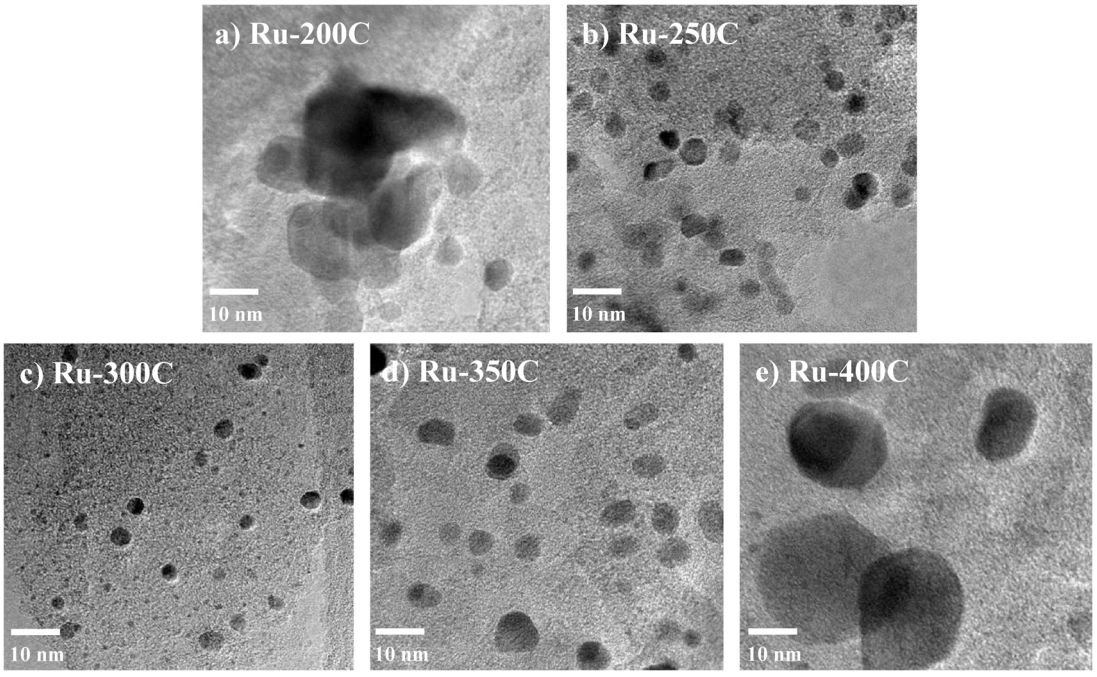

Fig. 4. HR-TEM images of Ru–*XC* catalysts reduced at 450 °C.

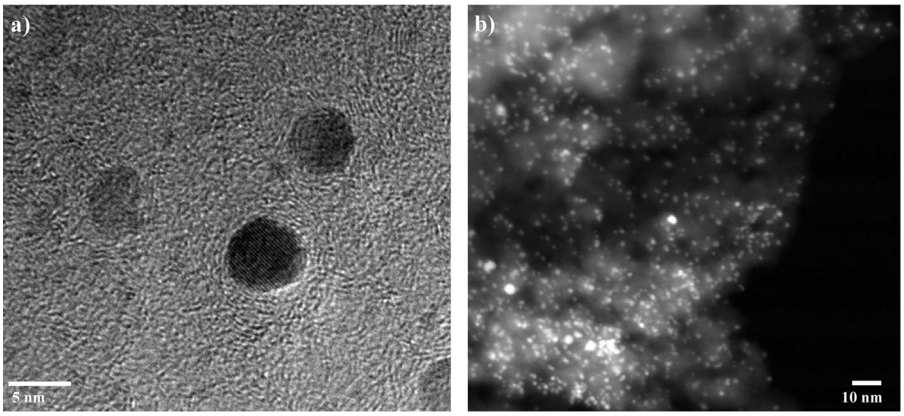

Fig. 5. (a) HR-TEM image of reduced Ru-300C catalyst and (b) its EDX image obtained by mapping on ruthenium.

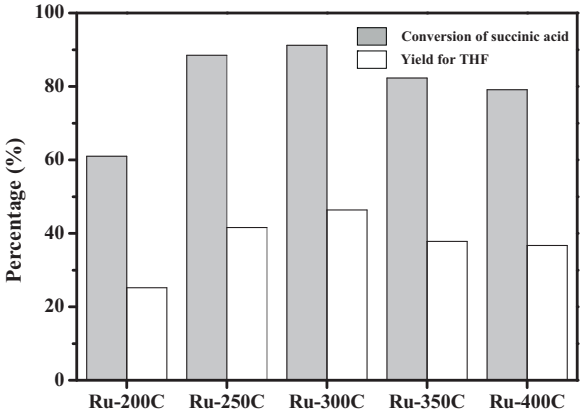

Fig. 6. Catalytic performance of Ru–*X*C catalysts in the liquid-phase hydrogenation of succinic acid to THF (reaction temperature = 240 °C, reaction pressure = 80 bar, reaction time = 4 h).

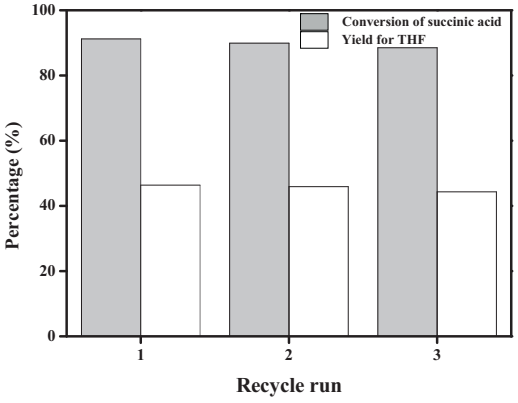

Fig. 8. Result for liquid-phase hydrogenation of succinic acid over Ru-300C catalyst with respect to recycle run (reaction temperature = 240 °C, reaction pressure = 80 bar, reaction time = 4 h).

of succinic acid (61.0%) and the lowest yield for THF (25.2%). It is believed that the excellent catalytic performance of Ru-300C catalyst was due to the smallest ruthenium particle size.

In order to investigate the effect of ruthenium particle size of Ru–*X*C (*X* = 200, 250, 300, 350, and 400 °C) catalysts on the catalytic activity in the hydrogenation of succinic acid, a correlation between ruthenium particle size of Ru–*X*C catalysts and yield for THF was established. Fig. 7 shows the correlation between ruthenium particle size of Ru–*X*C catalysts (determined by XRD) and yield for THF in the hydrogenation of succinic acid. The correlation clearly shows that yield for THF increased with decreasing ruthenium particle size (with increasing ruthenium dispersion) of Ru–*X*C catalysts. This result strongly supports that ruthenium particle size of Ru–*X*C catalysts served as an important factor determining the catalytic performance in the hydrogenation of succinic acid to THF.

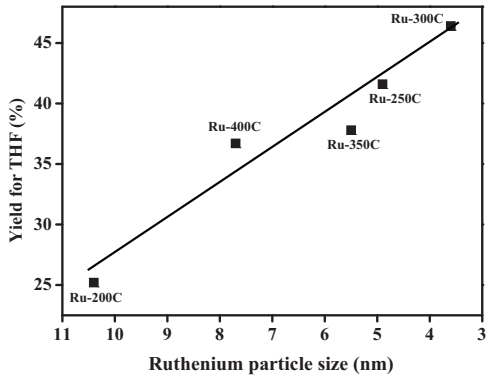

Fig. 7. A correlation between ruthenium particle size of Ru–*X*C catalysts and catalytic activity in the hydrogenation of succinic acid to THF.

3.4. Stability and reusability of Ru–XC catalyst

To investigate the stability and reusability of the catalyst, recycle tests for hydrogenation of succinic acid over Ru-300C catalyst were performed three times. Fig. 8 shows the result for liquid-phase hydrogenation of succinic acid to THF over Ru-300C catalyst with respect to recycle run. It was found that both fresh and spent catalysts showed similar catalytic activity (more than 95% of recycle efficiency). Furthermore, no significant ruthenium leaching (less than 1.0 ppm) was detected by ICP-AES analysis after each reaction test. Thus, Ru-300C catalyst served as a stable and reusable catalyst in the liquid-phase hydrogenation of succinic acid to THF.

4. Conclusions

Ruthenium–carbon composite (Ru–*X*C) catalysts prepared by a surfactant-templating method were pre-graphitized at different temperature (*X* = 200, 250, 300, 350, and 400 °C), and they were applied to the liquid-phase hydrogenation of succinic acid to THF. Among the Ru–*X*C (*X* = 200, 250, 300, 350, and 400 °C) catalysts, Ru-300C catalyst showed the smallest ruthenium particle size due to both moderate ruthenium–carbon interaction and well developed mesoporous structure. In the hydrogenation of succinic acid, both conversion of succinic acid and yield for THF showed

volcano-shaped trends with respect to pre-graphitization temperature; an optimal pre-graphitization temperature for the treatment of Ru–*X*C composites was required to achieve maximum yield for THF. Yield for THF in the hydrogenation of succinic acid increased with decreasing ruthenium particle size of Ru–*X*C catalysts. Thus, ruthenium particle size played a key role in determining the catalytic performance in the hydrogenation of succinic acid to THF over Ru–*X*C catalysts. In the recycle test, Ru-300C catalyst served as a stable and reusable catalyst for hydrogenation of succinic acid to THF.

Acknowledgements

This subject is supported by Korea Ministry of Environment as "Converging Technology Project (202-091-001)"

References

[1] J. Keneta, T. Asano, S. Masamune, Ind. Eng. Chem. 62 (1970) 24–32.
[2] V. Pallassana, M. Neurok, G. Coulston, Catal. Today 50 (1999) 589–601.
[3] S.P. Müller, M. Kucher, C. Ohlinger, B. Kraushaar-Czarnetzkyi, J. Catal. 218 (2003) 419–426.
[4] S.M. Jung, E. Godard, S.Y. Jung, K.-C. Park, J.U. Choi, J. Mol. Catal. A 198 (2003) 297–302.
[5] S.E. Hunter, C.E. Ehrenberger, P.E. Savage, J. Org. Chem. 71 (2006) 6229–6239.
[6] M.D. Wildberger, M. Maciejewski, J.-D. Grunwaldt, T. Mallat, A. Baiker, Appl. Catal. A 179 (1999) 189–202.
[7] B.K. Ly, D.P. Minh, C. Pinel, M. Besson, B. Tapin, F. Epron, C. Especel, Top. Catal. 55 (2012) 466–473.
[8] C. Delhomme, D. Weuster-Botz, F.E. Kühn, Green Chem. 11 (2009) 13–26.
[9] A. Cukalovic, C.V. Stevens, Biofuels Bioprod. Bioref. 2 (2008) 505–529.
[10] I. Bechthold, K. Bretz, S. Kabasci, R. Kopitzky, A. Springer, Chem. Eng. Technol. 31 (2008) 647–654.
[11] C. Du, S.K.C. Lin, A. Koutinas, R. Wang, C. Webb, Appl. Microbiol. Biotechnol. 76 (2007) 1263–1270.
[12] L. Rosi, M. Frediani, P. Frediani, J. Org. Chem. 695 (2010) 1314–1322.
[13] R. Luque, J.H. Clark, K. Yoshida, P.L. Gai, Chem. Commun. (2009) 5303–5307.
[14] U.G. Hong, H.W. Park, J. Lee, S. Hwang, I.K. Song, J. Ind. Eng. Chem. (2012) 462–468.
[15] P. Kim, J.B. Joo, W. Kim, J. Kim, I.K. Song, J. Yi, Catal. Lett. 112 (2006) 213–218.
[16] H. Kim, J.C. Jung, D.R. Park, S.-H. Baeck, I.K. Song, Appl. Catal. A 320 (2007) 159–165.
[17] U.G. Hong, D.R. Park, S. Park, J.G. Seo, Y. Bang, S. Hwang, M.H. Youn, I.K. Song, Catal. Lett. 132 (2009) 377–382.
[18] U.G. Hong, H.W. Park, J. Lee, S. Hwang, J. Yi, I.K. Song, Appl. Catal. A 415/416 (2012) 141–148.
[19] C.H. Yun, Y.H. Park, C.R. Park, Carbon 39 (2001) 559–567.
[20] M. Kruk, K.M. Kohlhaas, B. Dufour, E.B. Celer, M. Jaroniec, K. Matyjaszewski, R.S. Ruoff, T. Kowalewski, Microporous Mesoporous Mater. 102 (2007) 178–187.
[21] K.S.W. Sing, D.H. Everett, R.A.W. Haul, L. Moscou, R.A. Pierotti, J. Rouquérol, T. Siemieniewska, Pure Appl. Chem. 57 (1985) 602–619.
[22] J. Guo, A.C. Lua, J. Therm. Anal. Calorim. 60 (2000) 417–425.
[23] Z.Q. Li, C.J. Lu, Z.P. Xia, Y. Zhou, Z. Luo, Carbon 45 (2007) 1686–1695.
[24] Z.-Z. Lin, T. Okuhara, M. Misono, J. Phys. Chem. 92 (1988) 723–729.
[25] P. Betancourt, A. Rives, R. Hubaut, C.E. Scott, J. Goldwasser, Appl. Catal. A 170 (1998) 307–314.
[26] P.C.H. Mitchell, A.J. Ramirez-Cuesta, S.F. Parker, J. Tomkinson, D. Thompsett, J. Phys. Chem. 107 (2003) 6838–6845.
[27] C. Prado-Burguete, A. Linares-Solano, F. Rodríguez-Reinoso, C. Salinas-Martínez De Lecea, J. Catal. 128 (1991) 397–404.
[28] J. Okal, M. Zawadzki, L. Kępiński, L. Krajczyk, W. Tylus, Appl. Catal. A 319 (2007) 202–209.
[29] P. Scherrer, Göttinger Nachr. Ges. 2 (1918) 98–100.
[30] A.L. Patterson, Phys. Rev. 56 (1939) 978–982.
[31] Y. Bang, S.J. Han, J. Yoo, J.H. Choi, K.H. Kang, J.H. Song, J.G. Seo, J.C. Jung, I.K. Song, Int. J. Hydrogen Energy 38 (2013) 8751–8758.
[32] Z. Li, X. Hu, L. Zhang, S. Liu, G. Lu, Appl. Catal. A 417-418 (2012) 281–289.
[33] S.D. Robertson, B.D. McNicol, J.H. de Baas, S.C. Kloet, J. Catal. 37 (1975) 424–431.
[34] J.F. Le Page, Applied Heterogeneous Catalysis: Design, Manufacture, Use of Solid Catalysts, Editors Technip, Paris, 1987, pp. 357–434.
[35] H.S. Broadbent, Ann. N.Y. Acad. Sci. 145 (1967) 58–71.